In-plane response of slender walls made of calcium silicate brick and element masonry

R. Esposito, G.J.P. Ravenshorst, J.G. Rots

Faculty of Civil Engineering and Geosciences, Delft University of Technology, the Netherlands

Due to the increase of induced seismic activities in the Groningen area (north part of the Netherlands), the assessment of low-rise residential buildings with slender façade piers became of relevance. In this framework, the in-plane response of slender walls made of calcium silicate (CS) brick and element masonry is investigated in this paper. In-plane tests on full-scale masonry walls are presented along with a summary of an extensive material testing campaign. Despite the slenderness of the walls, uncommon for earthquake prone regions, the walls show a high ductility and displacement capacity typical of walls failing in rocking. Nevertheless, the finally brittle failure of CS element masonry walls is unfavourable with respect to the more gradual softening failure behaviour of CS brick masonry wall. This brittle failure may be related to the large size of the elements, 40 times bigger than the bricks, which promoted the faster development of splitting cracks in the units.

Keywords: Calcium silicate (CS) masonry, brick masonry, element masonry, seismic assessment, in-plane behaviour, Dutch masonry

1   Introduction

Nowadays calcium silicate (CS) masonry is widely used in the Netherlands and other north European countries, especially for the construction of low-rise residential buildings. As for other types of unreinforced masonry (URM), CS masonry units can be found in different sizes from small bricks, which can be laid by hand, to large elements, which are installed by using crane (Figure 1). Bricks were mainly used from the Second World War to the 80's, while the use of larger blocks and elements started from 1980.

Due to the increase of the induced seismic activity in the northern part of the Netherlands (Groningen region), the assessment of low-rise residential buildings became a relevant

topic. Among others, terraced houses represented one of the most vulnerable building typology largely spread over the area (Figure 2). Terraced houses often present a load-bearing inner leaf structure made of CS masonry.

Due to the fact that CS masonry was used mainly in countries not prone to natural seismic hazard, the characterisation of its material and structural behaviour within the framework of earthquake engineering is limitedly reported in literature. In the past, Dutch researchers studied the behaviour of CS brick and element masonry (van der Pluijm 1999, Vermeltfoort 2008); however they did not focus on aspects related to the seismic load. On the other hand, European researchers in the field of earthquake engineering generally focussed on block masonry having a thickness larger than typical Dutch units, e.g. 100 mm. (Anthoine and Molina 2008, Degée et al. 2008, Mayer and Caballero Gonzaléz 2008, Salmanpour et al. 2015).

(a)   *(b)*
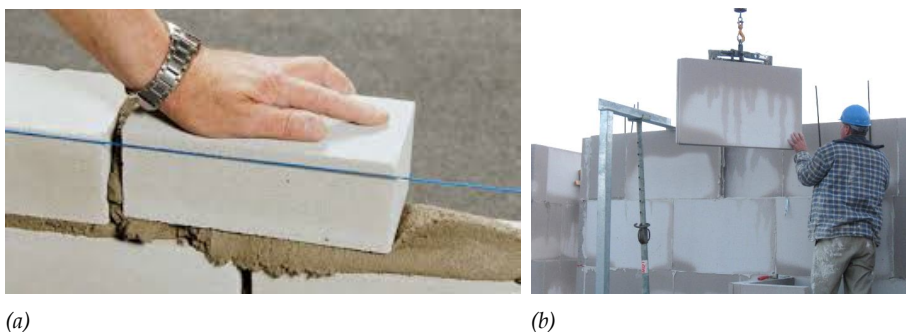
Figure 1. Construction of CS masonry: (a) bricks; (b) elements (VNK)

Figure 2. Typical Dutch terraced house (Esposito et al. 2019)

With the aim of supporting the seismic vulnerability assessment of low-rise buildings in the Groningen region, an extensive experimental campaign for the characterisation of CS brick and element masonry residential buildings has been carried out at the Macrolab or Stevinlaboratory of Delft University of Technology (Messali et al. 2017, Damiola et al. 2018, Esposito et al. 2018, Jafari et al. 2018, Messali et al. 2018, Esposito et al. 2019). A multiscale experimental campaign has been performed for the characterisation at material, component and structural level. For more information the reader can visit the website Structural Response to Earthquakes (www.tudelft.nl/citg/structural-response-to-earthquakes). This paper focuses on the behaviour at component level by analysing the results on in-plane shear-compression tests on full-scale walls. An overview of the main material properties is given in Section 2. Experimental tests on three slender walls in CS masonry, representing typical façade piers in terraced houses, are presented in Section 3. A comparison in terms of force and displacement capacity is given in Section 4. Eventually, conclusions are drawn in Section 5.

2 Materials and methods

2.1 Material characterisation

The material properties of CS masonry were selected to represent Dutch masonry used in existing buildings. The nominal dimensions of CS brick and element units were 210 x 70 x 100 mm and 900 x 650 x 100 mm, respectively. In the latter case, the units were tailored to the wall's geometry and pre-cut in the factory. In both cases a pre-mixed cement-based mortar was used. The CS bricks were laid traditionally by hand with a joint thickness of 10 mm. The CS element masonry was built with thin layer mortar joints (2-3 mm) by using a crane. In both cases, half-overlap running bond was placed at the bottom of the wall, as done in practice to guarantee verticality. Due to the large size of the CS elements, a kicker layer composed of smaller units was used. To reduce the material variability, the construction materials were produced in a single production batch and stored in protected environment prior to use.

The compression, bending and shear properties of both CS masonry types were investigated in dedicated experimental campaigns. The specimens for material tests were built at the same time of the walls for the in-plane tests (Jafari and Esposito 2017, Jafari et al. 2018). The tests were mainly performed by following the European standard (i.e. EN 1052), but a displacement controlled procedure was adopted to obtain an indication of the

Table 1. Material properties of CS brick and element masonry

Material property		Symbol	Unit
Density		ρ	kg/m³
Compressive strength of mortar		f_m	MPa
Normalised compressive strength of CS unit		f_b	MPa
Compressive strength of masonry perpendicular to bed joints		f'_m	MPa
Elastic modulus of masonry in the direction perpendicular to bed joint evaluated	at 1/3 of maximum stress	E_1	MPa
	at 1/10 of maximum stress	E_2	MPa
	between 1/3 and 1/10 of max. stress	E_3	MPa
Compressive strength of masonry parallel to bed joints		$f'_{m,h}$	MPa
Elastic modulus of masonry in the direction parallel to bed joints evaluated	at 1/3 of maximum stress	$E_{1,h}$	MPa
	at 1/10 of maximum stress	$E_{2,h}$	MPa
	between 1/3 and 1/10 of max. stress	$E_{3,h}$	MPa
Out-of-plane masonry flexural strength parallel to bed joint		f_{x1}	MPa
Out-of-plane masonry flexural strength perpendicular to bed joint		f_{x2}	MPa
Flexural bond strength		f_w	MPa
Masonry (bed joint) initial shear strength		f_{v0}	MPa
Masonry (bed joint) shear friction coefficient		μ	-

*Value obtained in a previous experimental campaign (Esposito et al. 2016, Esposito 2019), where materials produced in the same production batch were used.

post-peak behaviour. Table 1 lists the mean material properties for the CS brick and element masonry and their constituents.

The CS element masonry showed a higher compressive strength and elastic modulus with respect to the CS brick masonry. In the pre-peak phase, the CS brick masonry showed a linear-elastic phase followed by a slight decrease of stiffness prior to reaching the peak stress, while the CS element masonry showed a linear behaviour. After the maximum stress was reached, a softening behaviour was observed for the CS brick masonry, while a brittle failure was reported for the CS element masonry (Fig. 3).

Table 1. Continued

CS brick (Built 8/2016)			CS element (Built 8/2016)			Testing standard
Average	C.o.V.	No. test	Average	C.o.V.	No. test	
1805			1824	0.02	22	
7.57	0.06	150	16.10	0.09	36	EN 1015-11
13.26	0.13	75	19.40	0.06	18	EN 772-1
6.35	0.05		13.93	0.07		
4972	0.11		8557	0.19		
8206	0.12	6	9256	0.29	6	EN 1052-1
4265	0.10		8313	0.15		
7.55*	0.02*		9.42	0.17		
2212*	0.30*		8416	0.17		Similar to EN
3583*	0.47*	6*	10524	0.15	6	1052-1
2081*	0.42*		7701	0.19		
0.26*	0.18*		0.58	0.14	5	EN 1052-2
0.55*	0.39*	6*	0.73	0.04	4	EN:1052-2
0.12	0.12	7	0.55	0.17	20	EN:1052-5
0.13	-	12	0.83	-		
0.50	-	12	1.49	-	11	EN 1052-3

The CS element masonry showed approximately 2 times higher values for the out-of-plane masonry flexural strengths and the flexural bond strength with respect to the CS brick masonry. Consequently, the bond between masonry unit and mortar can be considered stronger in the case of CS element masonry. Comparing the results with previous studies by van der Pluijm (1999), similar values are obtained for the CS brick masonry, while larger value are observed for the CS element masonry. As for the bond strength properties, also the initial shear properties of CS element masonry resulted relative higher compared with those of CS brick masonry.

2.2 Specimens' characteristics

In-plane shear compression tests were performed on three walls, one made of CS brick (TUD_COMP-20) and two made of CS element masonry (TUD_COMP-24, TUD_COMP-25). An overview of the specimens' geometry and boundary conditions is given in Table 2, together with the aspect ratio and shear ratio. The latter is defined as the ratio between the effective height H_0 and the length L_w of the wall, where the former is calculated as the distance between the zero moment section and the base of the wall.
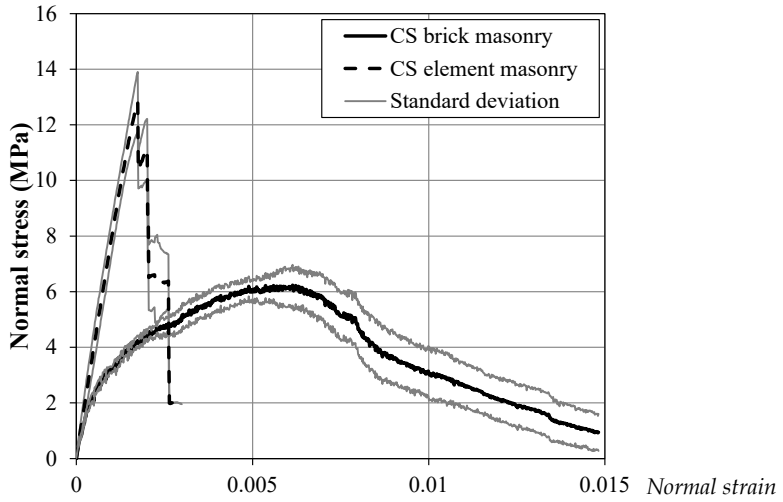
(a) Mean stress-strain curves and standard deviation

(b) CS brick masonry failure mode   *(c) CS element masonry failure mode*

Figure 3. Compression tests perpendicular to bed joints (adapted from Jafari et al. (2018))

Considering as reference the configuration of façade piers in typical terraced houses (Esposito et al. 2017, Graziotti et al. 2017, Esposito et al. 2018, Esposito et al. 2019), geometry and boundary conditions were defined. In terraced houses, the façade piers often represent the structural element contributing to define the global seismic behaviour of the structure for the weakest seismic loading direction. In this respect, their large slenderness ratio, which varies between 25 and 30, can be critical and it is also unusual with respect to the size of piers used in earthquake prone regions. The walls have similar height and thickness, but they differ in length due to the different construction detail that can be usually found between pier and transversal wall in a building. In the case of CS brick masonry buildings a running bond is present at pier-to-wall connection, while in the case of CS element masonry structures often a continuous vertical joint is used due to the large size of the units. Although the geometry of the facades is similar, the length of CS element masonry piers is shorter than the one of the CS brick masonry piers by the thickness of the transversal wall, i.e. 120 mm (Esposito et al. 2019).

Table 2. Characteristics of wall tested

Specimen name	Masonry type	Nominal dimensions	Aspect ratio	Pre-compression		Shear ratio	Boundary condition
		$L_w \times H_w \times t_w$	H_w/L_w	σ_v	σ_0/f_c'	H_0/L_w	
		mm	-	MPa	-	-	
TUD_COMP-20	CS brick	1110x2778x102	2.5	0.63	0.10	2.8	Cantilever
TUD_COMP-24	CS elem.	977x2743x100	2.8	0.60	0.04	1.4	Double clamped
TUD_COMP-25	CS elem.	977x2743x100	2.8	0.60	0.04	3.1	Cantilever

The CS element masonry walls were tested under double clamped (TUD_COMP-24) and cantilever configuration (TUD_COMP-25), while the CS brick masonry wall was tested under cantilever configuration (TUD_COMP-20). More information on the in-plane response of CS brick masonry walls can be found in Messali et al. (2017). A pre-compression stress σ_0 of 0.6 MPa was applied in every test. This value is typical for a façade pier located at the ground floor of a two story building with reinforced concrete floors when the rocking mechanism of the pier is activated.
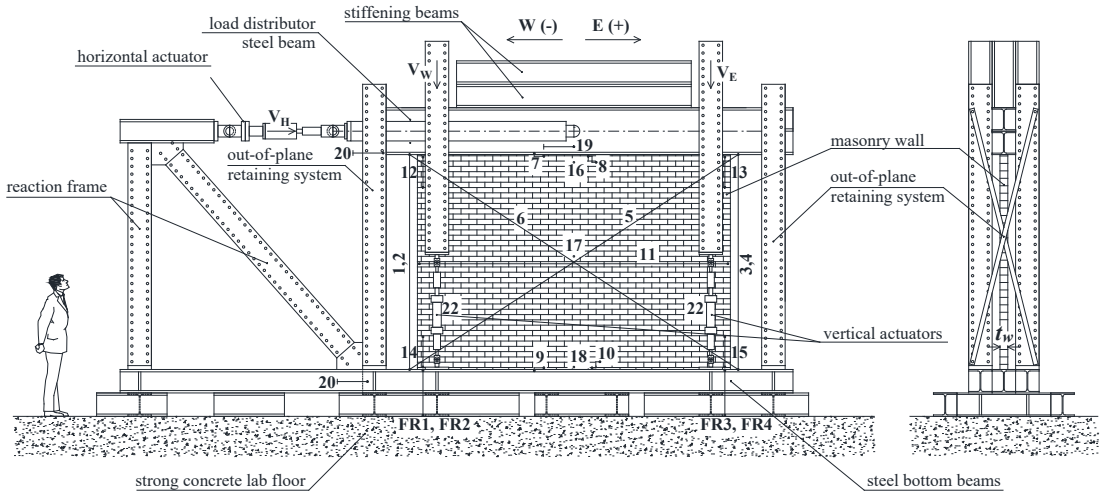
Figure 4. In-plane test set-up and measuring system (For sake of clarity the set-up is here presented for a squat wall with dimension 4000 x 2700 x 100 mm.)

2.3 Testing procedure

Figure 4 shows the in-plane test set-up and the measurement system adopted. A frame composed by a bottom and a top steel beam and two lateral steel column was used for the construction, transportation and testing of the wall. To prevent sliding between the masonry and the steel supporting beams, the first and last masonry courses were glued. The bottom steel beam is connected to cross-beams, which were anchored to the floor to prevent uplift. The top steel beam was used to introduce both the vertical and horizontal load to the masonry wall.

The set-up consists of a horizontal actuator and four vertical actuators. The horizontal actuator had a capacity of 400 kN and was connected at the centre of the top steel beam by means of steel tubes. For the pre-compression load, four vertical actuators with a capacity of each 100 kN were used and controlled pairwise. The vertical actuators were loaded in tension and were positioned by a steel frame on the top steel beam. The two steel frames of the vertical actuators helped in preventing undesired out-of-plane displacement of the top steel beam (Fig. 4). The vertical loading in the actuators could be differentiated to impose the cantilever or double clamped boundary conditions.

44

Linear potentiometers and lasers were used to measure the deformation of the wall (Fig. 4). To measure the net horizontal displacement of the wall two measurement systems were used. The first measuring system was composed of vertical (1-4) and diagonal (5-6) linear potentiometers installed between the top and bottom steel beam at the two side of the wall. The second measuring system consisted of two horizontal (19-20) and four vertical (FR1-FR4) sensors that measured the horizontal displacement of the steel beams and the possible rotation of the top flange of the bottom steel beam, respectively, with respect to external references. Differently than in the report by Esposito and Ravenshorst (2017), the net horizontal displacement of the wall was calculated with the second measurement system, because it was found more reliable for small deformations in the first cycles. A similar procedure was adopted by Messali et al. (2017). The drift has been calculated as the ratio between the net displacement at the top of the wall and the height of the wall H_w (Table 2). Sliding at the first and last mortar bed joints were measured by sensors 9 and 10; although not expected, possible sliding between the wall and the steel beams was measured with sensors 7 and 8. Horizontal deformations at the centre of the wall were measured by sensor 11. Possible cracking/crushing mechanisms due to flexural deformations were monitored with sensors 12-15 located at the corners of the wall over a length of 5 bricks. The absence of undesired out-of-plane deformation of the wall during the tests was monitored through the lasers 16-18. The forces were measured with load cells placed next to the hydraulic jacks (21-22).

The wall was subjected to a cyclic horizontal displacement, while a pre-compression load at the top of the wall was imposed. Every cycle was composed by three identical runs; in every run the desired target horizontal displacement was applied in both directions starting and ending at the zero position that is the initial position of the wall. A displacement-controlled procedure was applied by controlling the displacement of the horizontal jack. The loading rate per each cycle was first imposed to obtain a cycle's duration of 15 minutes until a maximum rate of 1 mm/s was reached and then kept constant. Table 3 lists the (measured) average drift per cycle in the first run.

To obtain the evaluation of the initial stiffness for different boundary conditions, a pre-test was performed in which the wall was subject to a cycle under cantilever configuration and one cycle under double clamped configuration. Both cycles had the same imposed horizontal target displacement similar to the one of cycle C1D.

3   Experimental results

Figure 5 shows the global response of the walls in terms of base shear versus drift curve and crack pattern observed in the last cycle. The graphs show the hysteretic behaviour, the backbone curve and its bilinear approximation. The backbone curve was defined by considering the maximum displacement achieved in each cycle (usually occurring in the first run) and its corresponding force. The evaluation of the equivalent bilinear curve is discussed in next section. An overview of the main experimental results is given in Table 4. The CS brick masonry wall tested under cantilever configuration (TUD_COMP-20) showed a rocking mechanism followed by toe crushing resulting in a gradual reduction of the force

Table 3. Measured average net horizontal displacement d and

average drift d_r in the first run of each cycle

Cycle	TUD_COMP-20		TUD_COMP-24		TUD_COMP-25	
	d	d_r	d	d_r	d	d_r
	mm	%	mm	%	mm	%
C1D	0.19	0.007	0.30	0.011	0.24	0.009
C2D	0.52	0.019	0.75	0.027	0.52	0.019
C3D	1.24	0.045	1.23	0.045	0.83	0.031
C1	1.23	0.044	1.25	0.046	0.98	0.036
C2	2.34	0.084	1.64	0.060	2.20	0.080
C3	3.61	0.13	2.68	0.098	3.45	0.126
C4	4.86	0.17	3.74	0.14	4.68	0.17
C5	9.90	0.36	7.37	0.27	9.69	0.35
C6	20.00	0.72	9.34	0.34	19.94	0.73
C7	30.45	1.10	15.92	0.58	30.17	1.10
C8	40.69	1.46	19.28	0.71	40.36	1.48
C9	51.04	1.84	26.12	0.96	50.64	1.85
C10	61.45	2.21	32.83	1.20	61.06	2.23
C11	71.97	2.59	39.53	1.45	75.24	2.75
C12	82.57	2.97	49.63	1.82	92.18	3.37
C13	90.29	3.25	66.60+	2.44+		
C14	90.17*	3.24*				

Cycle composed of 3.5 runs,   + Cycle composed of 2 runs
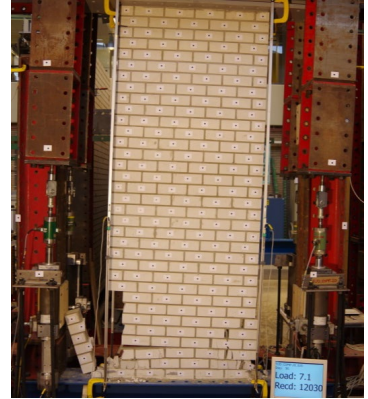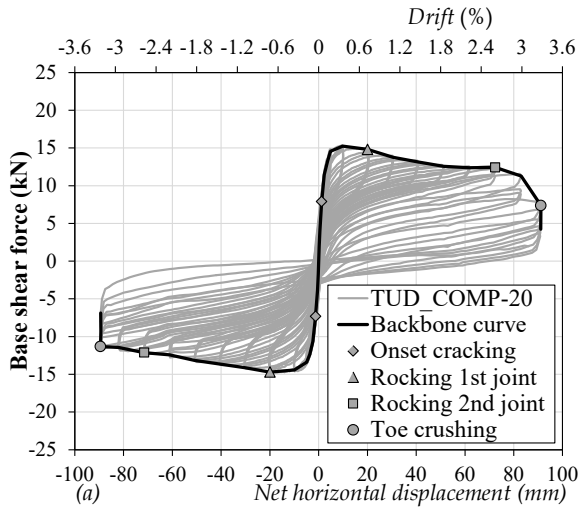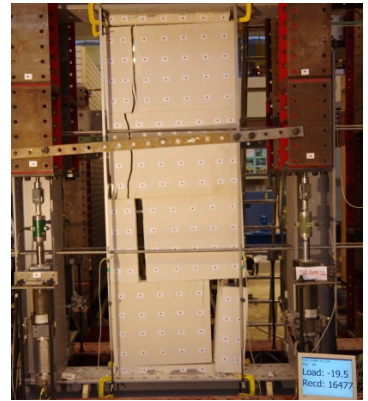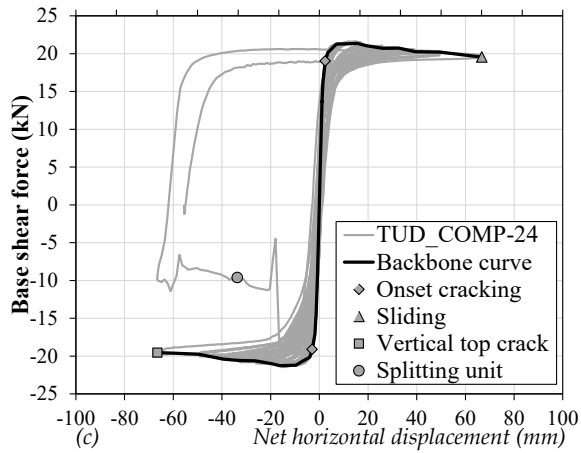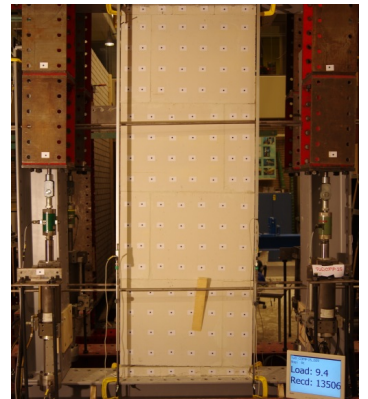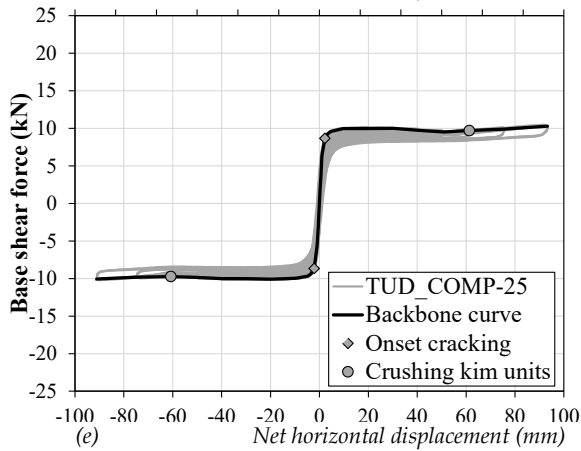
Figure 5. Hysteretic curve, envelope curve, equivalent bilinear curve and final crack pattern (corresponding approx. to circle marker): (a), (b) CS brick masonry wall TUD_COMP-20; (c), (d) CS element masonry wall TUD_COMP-24; (e), (f) CS element masonry wall TUD_COMP-25

capacity in the post-peak phase. During cycle C1, smaller horizontal cracks started to arise in the bottom three mortar layers and in cycle C6 the first mortar layer was completely damaged ensuring the full activation of the pure rocking mechanism. Due to the rocking deformation, the damage progressively involved the second bed joint at the bottom of the wall leading to the reduction of the effective height (cycle C11). During cycle C12, splitting cracks at the bottom-left and bottom-right corner of the wall occurred, leading to detachment of masonry portions on the left-hand side. In cycle C13 and C14, where the same jack's displacement was imposed, the phenomenon of toe crushing could be observed; the base shear force decreases substantially for the same imposed displacement. This phenomenon led to instability of the wall for large displacements and its complete collapse.

The CS element masonry wall tested under double clamped configuration (TUD_COMP-24) showed a pure rocking mechanism followed by a brittle failure with a sudden reduction of the force capacity. Upon cracking of the first and last bed joint (cycle C3), the wall deformed monolithically without showing any further damage. In the last cycle (cycle C13), brittle damage of the wall suddenly occurred in the following sequence: (i) sliding at the bottom two courses occurred leading to the head joint opening; (ii) formation of a vertical crack in the top two courses; (iii) splitting (over the thickness) of the bottom unit in the right-bottom corner. The sudden reduction in force capacity was determined by the formation of an unstable mechanism created by the cracking in the elements. This is in line with the brittle failure mechanism observed during the compressive tests (Fig. 3).

The CS element masonry wall tested under cantilever configuration (TUD_COMP-25) showed a pure rocking mechanism without degradation in force capacity. The damage

Table 4. Overview of experimental results in terms of initial stiffness K, maximum base shear force V, maximum net horizontal displacement d and maximum drift d_r

Specimen name	BCs*	K_c	K_{dc}	V^-	V^+	d^-	d^+	d_r^-	d_r^+
		kN/mm	kN/mm	kN	kN	mm	mm	%	%
TUD_COMP-20	C	9.0	13.9	-89.33	91.02	-3.21	3.27	-89.33	91.02
TUD_COMP-24	DC	5.3	12.4	-66.45	66.75	-2.43	2.45	-66.45	66.75
TUD_COMP-25	C	6.2	14.3	-91.09	93.27	-3.33	3.41	-91.09	93.27

*BCs = Boundary conditions, C = Cantilever, DC = Double clamped

48

started in cycle C2 with the formation of a horizontal crack at the first bed joint; the crack could reach a maximum crack opening of 25 mm leading to the monolithic deformation of the wall. Minor damage was also observed in the bottom kicker layer, where crushing was observed at the bottom-left and bottom-right corner starting from cycle C10. During the same cycle, out-of-plane deformation started and it reached a maximum value of 4 mm at the bottom of the wall. This resulted in a misalignment between the wall and the kicker layer. A similar phenomenon was also observed in the quasi-static cyclic test on full-scale two-storey building (Puente et al. 2018, Esposito et al. 2019). Despite the absence of relevant damage in the wall, the test was stopped due to the relative large drift value attained ($d_r > 3\%$).

4   Comparison in terms of in-plane response

In this Section, the experimental results are compared in terms of initial stiffness, residual displacement, hysteretic damping. Eventually, a comparison of the overall in-plane response is made by considering the equivalent bilinear approximation. For sake of clarity, the average net displacement is often used, which was calculated considering the absolute maximum value of the net displacement in positive and negative loading direction per each run.

4.1   Stiffness degradation

Figure 6 shows the normalised stiffness as a function of the normalised average net horizontal displacement. The stiffness was calculated considering a linear interpolation of the hysteretic curve for every cycle. The normalised value for the stiffness and the average net displacement were calculated by considering the initial stiffness in the first cycle (Table 4) and the ultimate displacement, respectively.

The CS brick masonry wall (TUD_COMP-20) shows a rapid degradation of the stiffness, while the curves for the CS element masonry walls (TUD_COMP-24 and TUD_COMP-25) show an initial plateau for the first four cycles. This difference can be related to the fact that after the first mortar joint was cracked, the CS element masonry wall showed a monolithic deformation associated to pure rocking. On the contrary, the CS brick masonry wall showed progressive cracking of the first two bed joints, which lead to a progressive reduction of the effective height. For larger deformation, the walls show a similar behaviour.

To evaluate the stiffness of the walls both in cantilever and double clamped configuration, cycle C1D was imposed prior to the cyclic test considering both boundary conditions (pre-test). Figure 6b shows the experimentally obtained value for the cantilever, K_c , and double clamped, K_{dc} , configuration and its ratio together with the theoretical value as per beam theory. The theoretical value has been calculated considering the elastic modulus evaluated at 1/10 of the compressive strength E_2 (Table 1) and assuming that the shear modulus G of masonry is 40% of its elastic modulus. Considering these assumptions, it is

(a)

Average net horizontal displacement – log_{10}

(b)
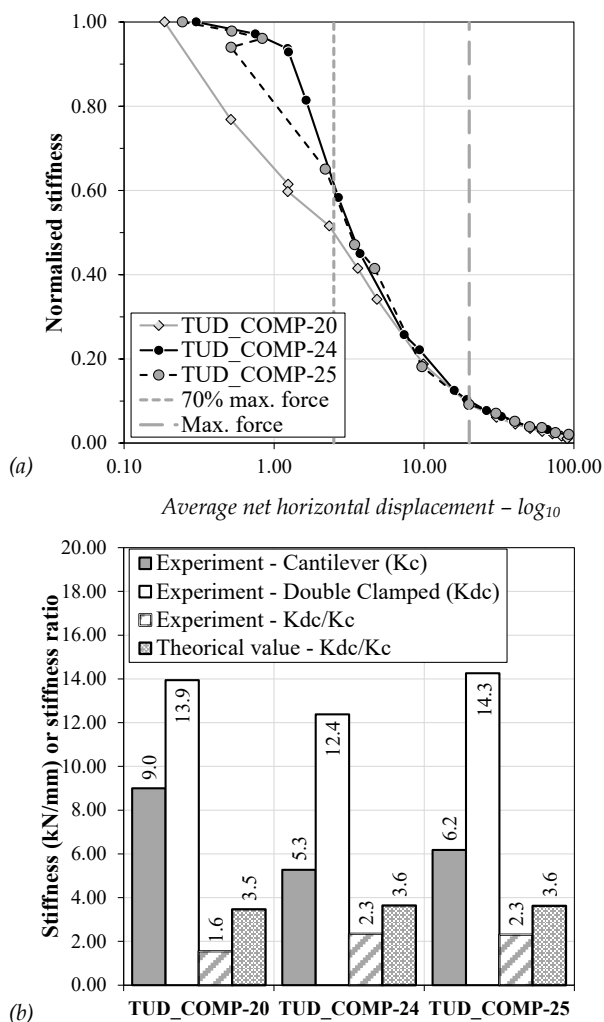
Figure 6. (a) Stiffness degradation; (b) Initial stiffness evaluated for cantilever and double clamped configuration (theoretical value calculated considering E_2 and $G = 0.4 E_2$)

possible to notice that the theoretical stiffness ratio is approximately 2 times higher than the one obtained experimentally.

4.2 *Residual displacement*

The walls showed large residual displacements. Figure 7 shows the normalised average residual displacement as a function of the average net horizontal displacement in the last (complete) run of each cycle, and the hysteretic curve for the cycle showing the largest residual displacement. The normalised residual displacement was calculated as the ratio between the displacement at zero force (residual displacement) and the peak displacement achieved in the corresponding half run. For sake of clarity, in Figure 7a the data is shown for drift value larger than 0.05% (cycle C3).

Prior to the formation of extensive crack pattern, for every wall the normalised residual displacement tends to a constant value of approximately 3%. The cantilever walls (TUD_COMP-20 and TUD_COMP-25) show a similar trend, while the double clamped wall (TUD_COMP-24) initially shows a normalised residual displacement 2 times lower than the cantilever walls.

For larger average net displacement, every wall shows an increase of residual displacements that can be associated to the damage evolution. For the CS brick masonry wall (TUD_COMP-20), a sudden increase in residual displacement is observed in the last two cycles (C13 and C14) where damage due to toe crushing was observed. Considering that in those cycles the wall shows similar net horizontal displacement, it is possible to notice that the toe crushing mechanism lead to an increase from approximately 22 to 46% in normalised residual displacement due to the repetition of similar runs. This phenomenon is also confirmed by the evolution in hysteretic behaviour shown in Figure 7b. For the CS element walls different behaviour is observed due to the substantial difference in crack pattern. For the double clamped wall TUD_COMP-24, which showed extensive damage, a sudden increase in normalised residual displacement is observed in the cycle with a residual displacement of approximatively 90% of the imposed one. Due to the absence of extensive damage in the masonry units for the cantilever wall TUD_COMP-25, the normalised residual displacement is nearly constant and an increase is observed only at drift value of 1.7% (Cycle C9) that is caused by sliding of the wall on the first bed joint, as can also be observed in the hysteretic curve in Figure 7b.
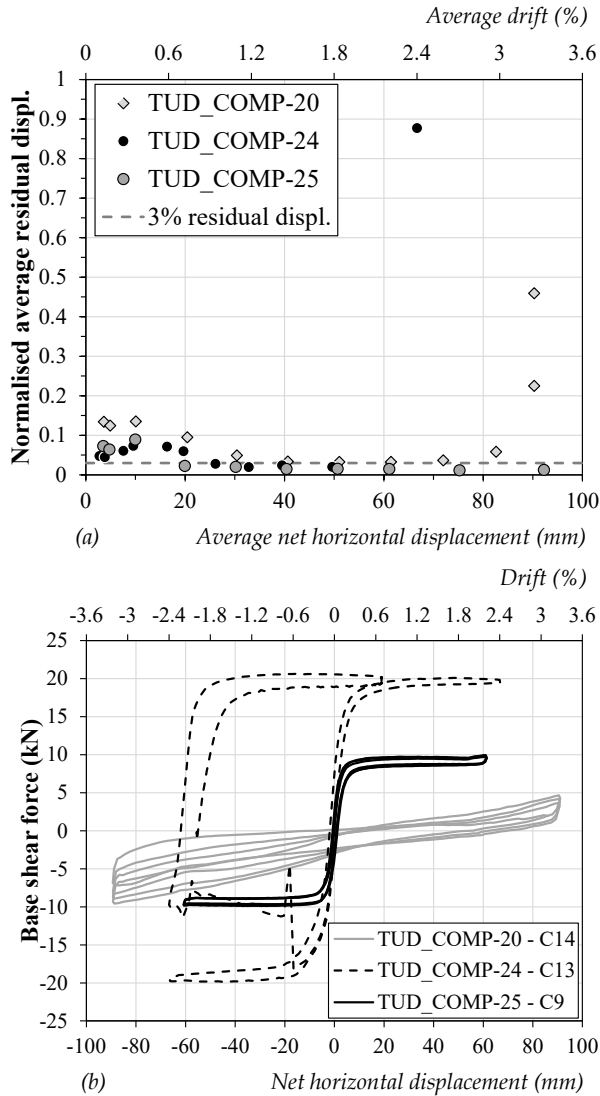
Figure 7. (a) Normalised average residual displacement in the last (complete) run of each cycle; (b) Cycle with the largest residual displacement

4.3 Hysteretic damping

To estimate the resistance to earthquakes in term of energy dissipation due to frictional mechanisms in the damaged state, an estimation of the hysteretic damping can be obtained from the quasi-static cyclic test. By considering the formulation first introduced by Jacobsen (1960) and reported by Priestley et al. (2007), the average hysteretic damping has

been calculated considering the area within one complete run of stabilized force-displacement response. Figure 8 shows the average hysteretic damping as a function of the average net displacement. To exclude the influence of possible friction in the actuators for low displacement, the value of hysteretic damping is given only for net horizontal displacements larger than 1 mm.
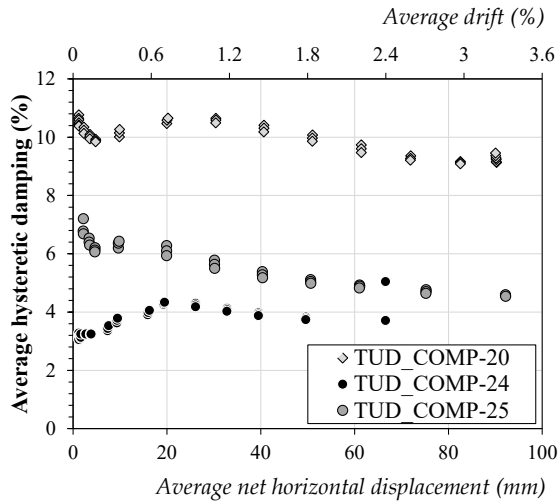
Figure 8. Hysteretic damping

The walls show a nearly constant trend for the average hysteretic damping as a function of the average net horizontal displacement. The CS brick masonry wall (TUD_COMP-20) shows the highest hysteretic damping being approximately 10%, while the CS element masonry walls show lower values, ranging between 4 and 5%. This difference can be related to the different damage mechanisms occurring for the two types of masonry. Thanks to the smaller unit size and the presence of thicker joints, the CS brick masonry can be considered more flexible with respect to the CS element masonry and it can dissipate more energy thanks to the activation of different local mechanisms such as splitting of brick, crushing of mortar, and sliding at mortar-brick interface. Additionally, the CS element masonry wall tested under cantilever configuration (TUD_COMP-25) shows a more pronounced initial degradation of the hysteretic damping with respect to the other two walls. For the double clamped CS element masonry wall (TUD_COMP-24), a sudden increase in hysteretic damping is observed in the last cycle as a consequence of the brittle damage.

4.4   Equivalent bilinear curve

To compare the performances of the walls in terms of force and displacement capacity, the equivalent bilinear approximation is adopted. The effective stiffness K_{eff} of the equivalent bilinear curve was evaluated at 70% of the maximum base shear force. The ultimate displacement d_u and its corresponding drift value $d_{r,b}$ were determined from the backbone curve at a residual force capacity equal to 80% of the maximum base shear force. The ultimate base shear force V_u of the equivalent bilinear curve was determined by imposing that the energy dissipated up to the ultimate displacement d_u is the same for the backbone and the equivalent bilinear curve. The elastic displacement d_{el} was calculated as the ratio between the ultimate base shear force and the effective stiffness (V_u/K_{eff}), while the ductility μ factor is calculated as the ratio between the ultimate and the elastic displacement (d_u/d_{el}). The main parameters of the bilinear approximation, obtained as average of the ones calculated for the negative and positive loading direction, are given in Table 5, while the equivalent bilinear curves for the two loading directions are shown in Figure 9.

Table 5. Parameters for the equivalent bilinear curve

Specimen name	BCs*	K_{eff}	d_{el}	d_u	μ	V_u	$d_{r,b}$
		kN/mm	mm	mm	-	kN	%
TUD_COMP-20	C	4.9	2.6	77.8	29.6	12.8	2.8
TUD_COMP-24	DC	11.1	1.8	66.6	36.8	20.1	2.4
TUD_COMP-25	C	3.9	2.5	92.2	37.1	9.8	3.4

*BCs = Boundary conditions, C = Cantilever, DC = Double clamped

The difference in crack pattern and energy dissipation of the two materials results relevant for the definition of the bilinear approximation. Due to the absence of progressive damage accumulation for the CS element masonry walls, the equivalent bilinear curve nearly resembles the backbone curve. On the contrary, the equivalent bilinear curve for the CS brick wall deviates approximately 10% from the backbone curve, both in terms of force and displacement capacity. In every case, the ductility factor is high confirming that the walls can withstand large deformation after the elastic phase. As already observed in Figure 6, the effective stiffness (Table 5) is approximately 50 and 85% of the initial stiffness (Table 4) for cantilever and double clamped configuration, respectively. However, the initial stiffness is evaluated for very small displacement thus it can be less representative of the structural response of the wall.
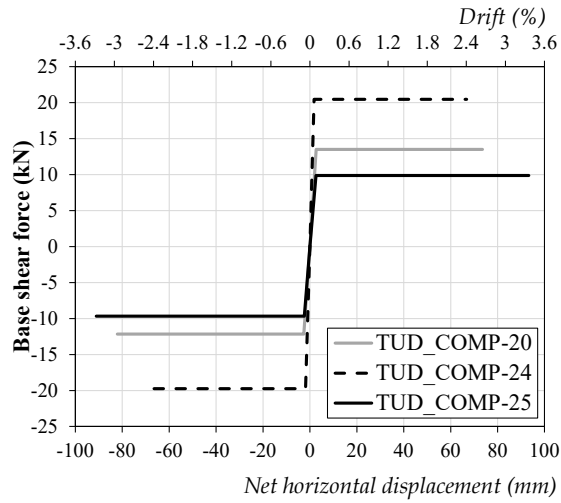
Figure 9. Equivalent bilinear curves

4.5 *Application of NPR 9998:2020*

The extensive experimental campaigns conducted at TU Delft in the past years, including the one presented in this paper, served as input for the development of the new Dutch standard NPR 9998:2020 (NEN 2020) for the assessment of unreinforced masonry buildings against induced seismicity.

Table 5 shows the comparison in terms of force and displacement capacity between the formulations proposed in NPR 9998:2020 and the values of the equivalent bilinear curve obtained in previous section (Table 5). Since the comparison is here made in terms of mean values, the NPR formulation for the drift limit, which calculates a characteristic drift value, has been modified accordingly as reported by Messali and Rots (Messali and Rots 2018,

Table 6. Force and displacement capacity accordingly to NPR 9998:2020 (NEN 2020)

Specimen name	BCs*	NPR 9998:2020			Bilinear curve		Error	
		V_{NPR}	$d_{r,NPR}$	Failure type	V_u	$d_{r,b}$	e_V	e_{dr}
		kN	%		kN	%	%	%
TUD_COMP-20	C	11.6	1.6	Flexural failure	12.8	2.8	10	42
TUD_COMP-24	DC	21.1	2.1	Splitting unit	20.1	2.4	-5	13
TUD_COMP-25	C	9.8	2.1	Flexural failure	9.8	3.4	0	37

*BCs = Boundary conditions, C = Cantilever, DC = Double clamped

2019). The NPR formulation is able to identify the correct failure mechanism and provides a good estimate in terms of base shear force, while a difference up to approximately 40% is observed for the ultimate drift. This difference can be ascribed to the large dataset adopted for the calibration of the NPR formulation, which considers a wide range of walls failing under rocking mechanisms with drift capacity ranging between 0.60 to 3.55%. The presented walls represent a minority within the dataset, thus explaining why the formulation provides a relative high error in the estimate of the displacement capacity.

5   Conclusions

Due to the increase of induced seismic activities in the Groningen area, the evaluation of the in-plane response of slender walls made of calcium silicate (CS) brick and element masonry became of relevance. They often represent the resisting structural elements determining the global response of terraced houses when loaded along their weak seismic direction. In this framework, the paper presents experimental results of in-plane shear-compression tests on full-scale slender walls made of CS masonry performed at Delft University of Technology as a part of larger experimental campaigns.

Due to their slenderness the walls show (as expected) a rocking failure mechanism and they can attain large displacement capacity. When considering similar boundary conditions, a difference of approximately 30% in base shear force is observed.

By considering the difference in masonry material, it is possible to note that the CS brick masonry wall showed gradual cracking up to the formation of the toe crushing mechanism, while the CS element masonry walls showed first a monolithic deformation as a rigid body followed in one case by a sudden brittle failure due to splitting of masonry unit. A similar difference in behaviour was observed also during the compressive tests on wallets, where a gradual post-peak softening behaviour occurred for the CS brick masonry, while brittle failure was attained for the CS element masonry upon reaching the maximum stress. Consequently, the CS brick masonry wall showed the highest stiffness degradation and the highest energy dissipation.

In conclusion, although the large CS element masonry units provide a monolithic rocking deformation of slender walls with a high ductility, the brittle failure mechanism associated to the splitting of compressed units and the limited energy dissipation is unfavourable in

the framework of earthquake engineering, especially considering the ultimate limit state. On the contrary, the gradual damage of CS brick masonry walls governed by crushing of the mortar bed joint and cracking of small units, can allow reaching comparable ultimate drifts with larger energy dissipation.

References

Anthoine, A. and Molina, F. (2008). Pseudo-dynamic testing of full scale masonry structures: preparatory work. Proc. 14th *International Brick and Block Masonry Conference*.

Damiola, M., Esposito, R., Messali, F. and Rots, J.G. (2018). Quasi-static cyclic two-way out-of-plane bending tests and analytical models comparison for URM walls. 10th *International Masonry Conference* (IMC). Milani, G., Taliercio, A. and Garrity, S. Milan, Italy.

Degée, H., Denoël, V., Candeias, P., Campos Costa, A. and Coelho, E. (2008). Experimental investigations on non-engineered masonry houses in low to moderate seismicity areas. Proceedings of the 14WCEE, 14th *World Conference on Earthquake Engineering*.

Esposito, R., Errata to tests for the characterization of replicated masonry and wall ties. 2019, C31B60-1E1, Delft University of Technology.

Esposito, R., Jafari, S., Ravenshorst, G.J.P., Schipper, H.R. and Rots, J.G. (2018). Influence of the behaviour of calcium silicate brick and element masonry on the lateral capacity of structures. 10th *Australasian Masonry Conference* (AMC). Sydney, Australia.

Esposito, R., Messali, F., Ravenshorst, G.J.P., Schipper, H.R. and Rots, J.G. (2019). Seismic assessment of a lab-tested two-storey unreinforced masonry Dutch terraced house. *Bulletin of Earthquake Engineering* 17(8): 4601-4623.

Esposito, R., Messali, F. and Rots, J., Tests for the characterization of replicated masonry and wall ties. 2016, C31B60-1, Delft University of Technology.

Esposito, R. and Ravenshorst, G., Quasi-static cyclic in-plane tests on masonry components 2016/2017. 2017, C31B67WP3-4, Delft University of Technology.

Esposito, R., Terwel, K., Ravenshorst, G., Schipper, H., Messali, F. and Rots, J. (2017). Cyclic pushover test on an unreinforced masonry structure resembling a typical Dutch terraced house. 16th *World Conference on Earthquake* (WCEE). Santiago, Chile.

Graziotti, F., Tomassetti, U., Kallioras, S., Penna, A. and Magenes, G. (2017). Shaking table test on a full scale URM cavity wall building. *Bulletin of Earthquake Engineering* 15(12): 5329-5364.

Jacobsen, L.S. (1960). Damping in composite structures. 2nd *World Conference on Earthquake Engineering* (WCEE). Tokyo and Kyoto, Japan. 2: 1029-1044.

Jafari, S. and Esposito, R., Material tests for the characterisation of replicated calcium silicate element masonry. 2017, C31B67WP1-11, Delft University of Technology.

Jafari, S., Esposito, R. and Rots, J.G. (2018). From Brick to Element: Investigating the Mechanical Properties of Calcium Silicate Masonry. 11th *international conference on Structural Analysis of Historical Constructions* (SAHC). Cusco, Peru.

Mayer, U. and Caballero Gonzaléz, A. (2008). ESECMaSE – Shaking table tests at the national technical university in Athens. 14th *International Brick and Block Masonry Conference*. Sydney, Australia.

Messali, F., Esposito, R., Jafari, S., Ravenshorst, G.J.P., Korswagen, P. and Rots, J.G. (2018). A multiscale experimental characterisation of Dutch unreinforced masonry buildings. 16th *European Conference on Earthquake Engineering* (ECEE). Thessaloniki, Greece: 18-21.

Messali, F., Ravenshorst, G.J.P., Esposito, R. and Rots, J.G. (2017). Large-scale testing program for the seismic characterization of Dutch masonry walls. 16th *World Conference of Earthquake Engineering* (WCEE). Santiago, Chile.

Messali, F. and Rots, J.G. (2018). In-plane drift capacity at near collapse of rocking unreinforced calcium silicate and clay masonry piers. *Engineering Structures* 164: 183-194.

Messali, F. and Rots, J.G. (2021). Definition of the near collapse in-plane drift capacity of rocking unreinforced masonry walls for the Dutch national guidelines, *Heron* Vol. 66, No. 1 (2021) pp. 19-36.

NEN (2020). NPR 9998 - Assessment of structural safety of buildings in case of erection, reconstruction and disapproval - Induced earthquakes - Basis of design, actions and resistances. Delft, The Netherlands, Nederlands Normalisatie-instituut.

Priestley, M.J.N., Calvi, G.M. and Kowalsky, M.J. (2007). *Displacement-Based Seicmic Design of Structures*. Eds. Pavia, Italy, IUSS Press.

Puente, I., Lindenbergh, R., van Natijne, A., Esposito, R. and Schipper, H.R. (2018). Monitoring of progressive damage in buildings using laser scan data ISPRS Technical Commission II Symposium 2018, Riva del Garda, Italy.

Salmanpour, A.H., Mojsilović, N. and Schwartz, J. (2015). Displacement capacity of contemporary unreinforced masonry walls: an experimental study. *Engineering Structures* 89: 1-16.

van der Pluijm, R., Out-of-plane bending of masonry: behaviour and strength. 1999, Eindhoven University of Technology.

Vermeltfoort, A. (2008). Mechanical properties and application features of CASIELS. Proceedings of the 14th *International Brick and Block Masonry Conference*.

VNK. Retrieved 06/06/2019, from www.vnk.nl.